Available online at www.springerlink.com

Acta Metall. Sin. (Engl. Lett.) Vol.26 No. 5 pp. 497—502 October 2013

ACTA
METALLURGICA SINICA
(ENGLISH LETTERS)

Optimization of Grain Boundary Character Distribution in Fe-18Cr-18Mn-0.63N High-Nitrogen Austenitic Stainless Steel

Feng SHI[1)], *Xiaowu LI*[1)†], *Yutong HU*[1)], *Chuan SU*[1)] *and Chunming LIU*[2)]

1) Institute of Materials Physics and Chemistry, College of Sciences, Northeastern University, Shenyang 110819, China

2) School of Materials and Metallurgy, Northeastern University, Shenyang 110819, China

[Manuscript received 29 May 2013, in revised form 19 June 2013]

Grain boundary engineering (GBE) is a practice of improving resistance to grain boundary failure of the material through increasing the proportion of low Σ coincidence site lattice (CSL) grain boundaries (special grain boundaries) in the grain boundary character distribution (GBCD). The GBCD in a cold rolled and annealed Fe-18Cr-18Mn-0.63N high-nitrogen austenitic stainless steel was analyzed by electron back scatter diffraction (EBSD). The results show that the optimization process of GBE in the conventional austenitic stainless steel cannot be well applied to this high-nitrogen austenitic stainless steel. The percentage of low ΣCSL grain boundaries could increase from 47.3% for the solid solution treated high-nitrogen austenitic stainless steel specimen to 82.0% for the specimen after 5% cold rolling reduction and then annealing at 1423 K for 10 min. These special boundaries of high proportion effectively interrupt the connectivity of conventional high angle grain boundary network and thus achieve the GBCD optimization for the high-nitrogen austenitic stainless steel.

KEY WORDS: High nitrogen austenitic stainless steel; Grain boundary character distribution; CSL grain boundary; EBSD

1. Introduction

High-nitrogen austenitic stainless steels (HNASS) own not only low cost but also excellent mechanical properties, corrosion resistance, oxidization resistance, wearability, *etc.*[1−5]. However, the high nitrogen content may cause the precipitation of nitride during welding in HNASS. The results reported by Ogawa *et al.*[6] indicated that the precipitation of nitride would occur in 23Cr-4Ni-2Mo-1N HNASS when it was subjected to between 1173 K and 1373 K for 2 s. Thus, it is difficult to avoid the precipitation in HNASS during welding. The nitride precipitation can cause serious intergranular corrosion tendency in the heat affected zone (HAZ), which directly limits the practical applications of such advanced ferrous materials.

Recent studies on grain boundary structure indicated that intergranular corrosion depends strongly on crystallographic nature and atomic structure of the grain boundary, and the low energy grain boundaries such as low Σ coincidence site lattice (CSL) grain boundaries (special grain boundaries) have strong resistance to intergranular corrosion[7,8]. While grain boundary engineering (GBE) is such a method of enhancing resistance to grain boundary failure of the material through increasing the proportion of low Σ CSL grain boundaries in the grain boundary character distributions (GBCD).

In recent years, GBE has been widely used as a new way to solve the grain boundary failure problems including intergranular corrosion[9−11]. At present, some research progress in the GBCD optimization of the conventional austenitic stainless steels (ASS) has been made[12,13], focusing mainly on 304 ASS[9,10,14−16] and partially on 304L, 316 and 316L ASS[17−19]. However, there are as yet few reports on

† Corresponding author. Prof., Ph.D.; Fax: +86 24 83678479; E-mail address: xwli@mail.neu.edu.cn (Xiaowu LI)

DOI: 10.1007/s40195-013-0323-5

the GBCD optimization in HNASS. In the present work, GBCD of Fe-18Cr-18Mn-0.63N HNASS was investigated in order for probing into the practicability of GBE method to such an advanced ferrous material.

2. Experimental

The experimental steel used in the present study was melted by induction furnace and electroslag remelting (ESR) furnace both filled with N_2, and cast into water-cooled mould. After forged at 1473 K, the cast ingot was hot-rolled at 1373 K into a plate with 6 mm thickness and then cold rolled into plates with 4 mm thickness. The chemical composition of the steel was analyzed to be 17.97 wt.% Cr, 18.0 wt.% Mn, 0.63 wt.% N, 0.056 wt.% C, and 0.02 wt.% Al and Fe is the bal.. The cold-rolled plates were hold at 1323 K for 1 h followed by water quenching (hereafter referred to as solid solution treatment). The solution-treated specimen was termed here as base material (BM). The BM was cold-rolled by 3, 5 and 10% in thick reduction, and then respectively annealed at 1423 K for 5 min, 10 min, 1 h, 12 h, 24 h and 72 h, and at 1223 K for 10 min, 12 h, 24 h and 72 h in vacuum and quickly cooled in water. The GBCD of the specimens was examined by orientation imaging microscopy (OIM) system attached to a JEOL JSM 7001F field emission scanning electron microscope (FESEM). In order to ensure the statistical significance, the scanning area of the specimen is no less than 1.0 mm × 1.0 mm. The scanning step of 1 μm was adopted according to the grain size of the experimental steel. Grain boundaries with $1< \sum <29$ were regarded as coincidence site lattice (CSL) boundaries with low energy, and the others as random boundaries with high energy. For the electron back scatter diffraction (EBSD) measurements, the specimen surfaces were subsequently electro-polished in a solution of $HClO_4$: CH_3CH_2OH=8:100 (in volume ratio) under 30 V for 15 s.

3. Results and Discussion

Fig. 1 shows the GBCD of base metal (BM). The special boundaries (SBs) are shown in red and the conventional high angle boundaries (HABs) are shown in black. The fraction of special boundaries (f_{SB}) is determined to be 47.3% in BM. From Fig. 1, it can be obviously observed that the connectivity of the conventional HABs network is relatively complete.

Fig. 2 shows the effects of the cold-rolling reduction ratio and the annealing time at 1423 K on the f_{SB} in HNASS during the thermo-mechanical processing for GBE. Apparently, the f_{SB} in the specimens cold-rolled at 5% reduction ratio and annealed both for 10 min and 24 h are comparatively higher. The highest f_{SB} is obtained to be around 82.0% in the specimen cold-rolled at 5% reduction ratio and annealed at 1423 K for 10 min.

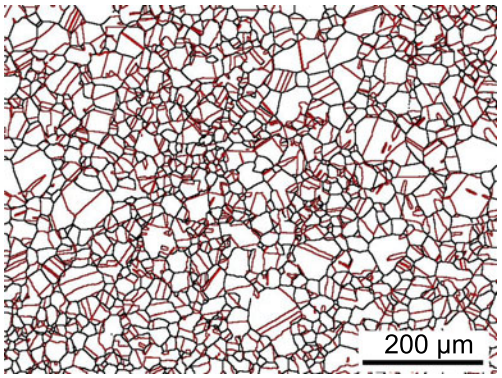

Fig. 1 EBSD image of reconstructed grain boundaries for the BM specimen of HNASS

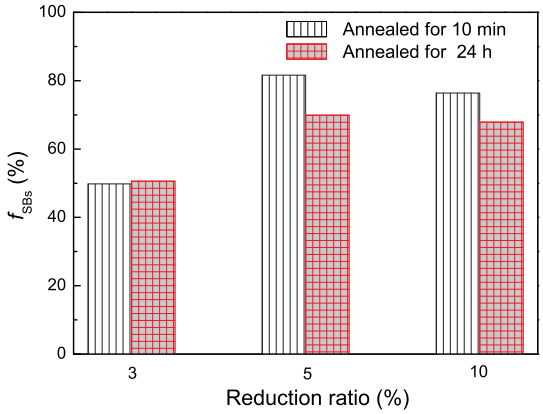

Fig. 2 Effects of the cold-rolling reduction ratio and the annealing time at 1423 K on the fraction of SBs in the HNASS

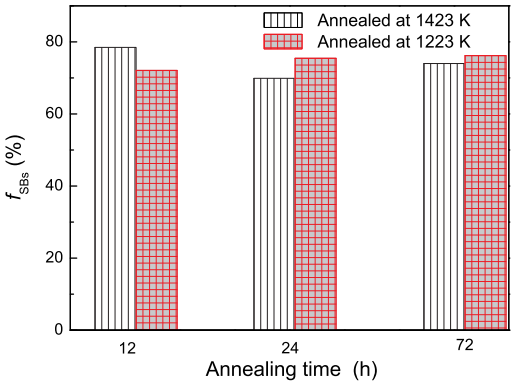

Fig. 3 Effects of the annealing time at 1423 K and 1223 K on the fraction of SBs in the HNASS

According to the results in Fig. 2, the EBSD measurements were further carried out on the specimens annealed at 1423 K and 1223 K for different times at 5% reduction ratio and the results are shown in Fig. 3. It is clear that the f_{SB} in the specimens annealed at 1423 K and 1223 K for longer time are all no more than 80%. Therefore, the f_{SB} is still the highest in the specimen cold-rolled at 5% reduction ratio and annealed at 1423 K for 10 min under the present

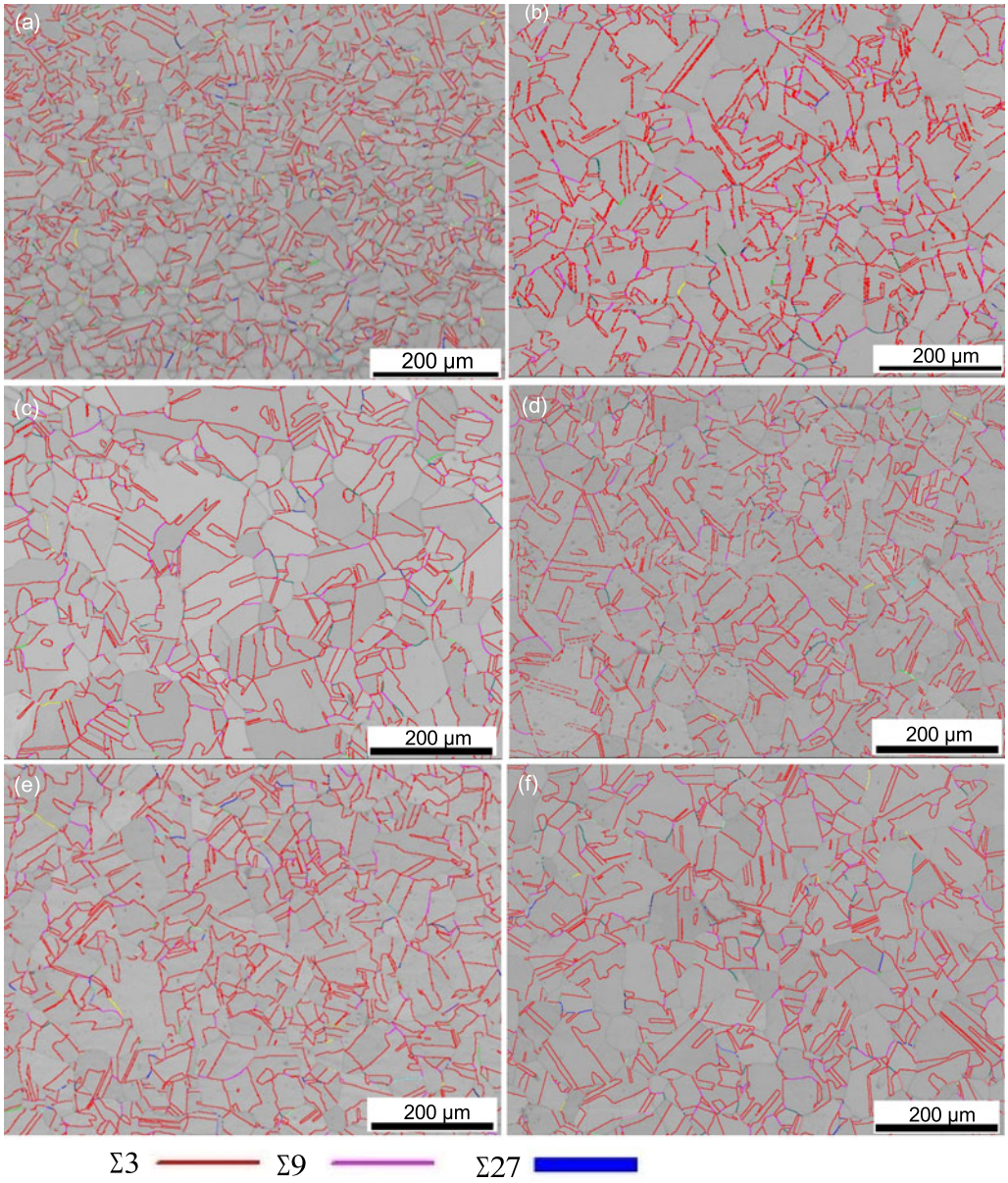

Fig. 4 EBSD reconstructed images of low CSL grain boundaries in the specimens cold-rolled by 5% and then annealed at 1423 K for different time: (a) 5 min; (b)10 min; (c)1 h; (d)12 h; (e) 24 h; (f) 72 h

Table 1 Proportions of various SBs for the BM specimen and specimens cold-rolled by 5% and then annealed at 1423 K for different time

Specimen	$\sum 3$ (%)	$\sum 9 + \sum 27$ (%)	Ratio of $(\sum 9+\sum 27)/\sum 3$	Other low CSL grain boundaries (%)	Total SBs (%)
BM	42.6	1.4	0.03	3.3	47.3
TM-5 min	36.1	1.3	0.04	3.1	40.5
TM-10 min	70.3	10.5	0.15	1.2	82.0
TM-1 h	62.0	9.0	0.14	2.0	73.0
TM-12 h	67.6	9.7	0.14	1.2	78.5
TM-24 h	60.2	7.7	0.13	2.1	70.0
TM-72 h	64.0	8.5	0.13	1.5	74.0

Note: TM means the specimen after cold-rolled and annealed

experimental conditions.

The EBSD-reconstructed images for low CSL grain boundaries and the proportions of various CSL grain boundaries for the specimens cold-rolled by 5% and then annealed at 1423 K for different times are respectively shown in Fig. 4 and Table 1. According to Fig. 4 and the data in Table 1, as with conventional ASS, the total SBs consist mainly of $\sum 3^n$ (n=1, 2, 3) grain boundaries, in addition to a small amount of other low CSL grain boundaries, and $\sum 3$ grain

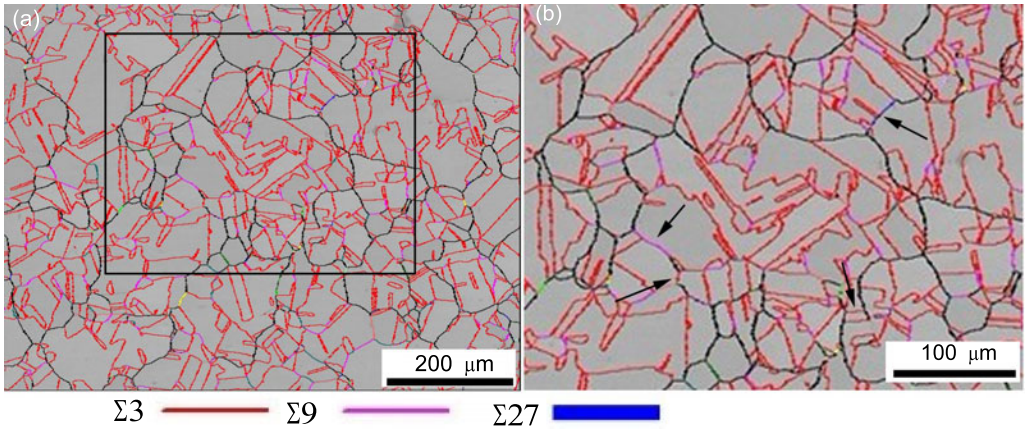

Fig. 5 EBSD image of reconstructed grain boundaries for the HNASS specimen cold-rolled by 5% at 1423 K for 10 min (a), and the partially enlarged detail of the square frame in Fig. 5(a) (b)

boundaries are dominant in SBs in HNASS. From Table 1, it can also be found that, not only the proportion of the $\sum 3$ grain boundaries, but also the proportions of $\sum 9+\sum 27$ and the ratio of $\sum 9+\sum 27$ to $\sum 3$ are all the highest in the specimen cold-rolled at 5% reduction ratio and annealed at 1423 K for 10 min.

To examine whether the optimization of GBCD has been truly realized in the material, the evaluation only by the proportion of low $\sum$ CSL grain boundaries is often insufficient. This is because GBCD of the material cannot achieve the optimization effect and will not play a role in resisting the failure behavior of the grain boundaries (*e.g.* intergranular corrosion and/or cracking), if SBs of high proportion locate inside the grain and do not interrupt the connectivity of the conventional HABs network[20−22].

Fig. 5 shows the grain boundary reconstruction from EBSD data for the specimen cold-rolled at 5% reduction ratio and annealed at 1423 K for 10 min. It is obvious that some clusters consisting mainly of SBs appear and effective disruption of the general HABs networks has been achieved as shown by the arrows in Fig. 5(b).

4. Discussion

The low $\sum$ CSL boundaries of high proportion can be obtained through GBE process of annealing at lower temperatures for long time in the conventional ASS[12,13]. The experimental results were provided by Shimada *et al.*[12] show that the f_{SB} rises from 63% in the BM to 86% in the 304 ASS cold-rolled by 5% and then annealed at 1200 K for 72 h, and an increase of 23% in the f_{SB} is achieved. Michiuchi *et al.*[13] made the similar GBE treatment to 316 ASS and obtained an increase of 31% in the f_{SB}, *i.e.*, increase from 55% to 86%. In contrast, in the present work, the f_{SB} rises from 47.3% in the BM to 82.0% in HNASS cold-rolled by 5% and then annealed at 1423K for 10 min, with an increase of 35% in f_{SB} being obtained. Provided that a similar GBE process with that of the conventional ASS, *e.g.* cold-rolling by 5% and then annealing at 1223 K for 72 h, was applied to the present HNASS, the f_{SB} can just reach 76%. Therefore, the optimization process of GBE in HNASS should be different from that in conventional ASS. In fact, the GBCD optimization is a very complicated process and it is generally affected by many factors, such as original grain size and orientation, original GBCD, *etc.* The GBCD optimization in ASS is achieved normally through deformation and thermo-mechanical processing. For the present HNASS, it has a lower stacking fault energy and higher stability, as compared to the conventional ASS, and cold deformation almost cannot induce a martensitic transformation in HNASS[23,24], so that the microstructure evolution as well as deformation behavior and micro-mechanism in HNASS are different from those in the conventional ASS. Correspondingly, the velocity, mode and driving force of grain boundary migration are also different during subsequent annealing. As a result, the optimization process of GBE in the conventional ASS is not well applicable for HNASS, while a small pre-strain and short-term annealing at higher temperature yielded an optimum GBCD for the formation of a high proportion of low CSL grain boundaries in the HNASS under the current experimental conditions. It should be mentioned that the f_{SB} in HNASS is not higher than that in the conventional ASS, this is because the f_{SB} of the BM is lower in this experimental steel. Although the absolute value of low CSL grain boundary proportion f_{SB} is not the highest in HNASS, as compared to 304 ASS[12] and 316 ASS[13], the relative increase of 35% is the largest. Furthermore, the SBs of high proportion effectively interrupt the connectivity of conventional HABs network, and the GBCD optimization effect is thus achieved (Fig. 5). So the GBE method applying to the present advanced ferrous material is practicable.

The GBE to improve the grain boundary characteristics has been categorized into four types by Wang and Zhou[25], based individually on annealing twins,

textures, in situ self-coordination and alloying, among which the annealing twin-based GBE applies specially to face centered cubic (fcc) metals and alloys with medium or low stacking fault energy, for which annealing twins can easily form during deformation and annealing. Concerning the optimization mechanism of twin-induced GBCD, there are currently four major modes: (1) Regenerating model of $\sum 3$ grain boundaries proposed by Randle[26], considering that HABs and coherent $\sum 3$ grain boundaries firstly react to generate $\sum 9$ grain boundaries, then the $\sum 9$ grain boundaries continue moving to react with the other coherent $\sum 3$ grain boundaries, eventually deriving incoherent $\sum 3$ grain boundaries to interrupt the connectivity of conventional HABs. (2) Decomposing model of high CSL grain boundary proposed by Kumur *et al.*[27], describing that the strain-induced boundary migration generates $\sum 3$ annealing twin boundaries, which further react with high CSL grain boundaries to generate a number of low CSL grain boundaries. For example, $\sum 51$ and $\sum 87$ react with $\sum 3$ to generate $\sum 17$ and $\sum 29$ grain boundaries, respectively. (3) Special fragmentation model proposed by Shimada *et al.*[12], stating that the GBCD optimization is achieved by introducing fragmentations of low energy SBs to the HABs. (4) Migrating and reaction model of incoherent $\sum 3$ grain boundary proposed by Wang and Zhou[25], declaring that the appearance of lots of incoherent $\sum 3$ grain boundaries (curved $\sum 3$ grain boundaries) during deformation and annealing is the origin for achieving GBCD optimization. These incoherent $\sum 3$ grain boundaries can derive $\sum 9$ and $\sum 27$ grain boundaries through the reactions of $\sum 3 + \sum 3 \rightarrow \sum 9$ and $\sum 3 + \sum 9 \rightarrow \sum 27$.

According to the above-described optimization mechanism of GBCD, the present experimental results in HNASS can well be explained by the migrating and reaction model of incoherent $\sum 3$ grain boundaries. A number of incoherent $\sum 3$ grain boundaries, *i.e.* the curved $\sum 3$ grain boundaries, can be clearly observed in the GBCD optimized specimens (*e.g.* see Fig. 5). The $\sum 9$ and $\sum 27$ grain boundaries are derived by lots of curved $\sum 3$ grain boundaries through grain boundary reactions according to the model proposed by Wang and Zhou[25], but the deriving capacity of $\sum 3$ grain boundaries is different according to the data in Table 1. The ratio of $(\sum 9 + \sum 27)/\sum 3$ describes the deriving capacity of $\sum 3$ grain boundaries to $\sum 9$ and $\sum 27$ ones[8]. From Table 1, it can be seen that the ratio of $(\sum 9 + \sum 27)/\sum 3$ increases from 0.03 in BM to 0.15 in the specimen cold-rolled at 5% reduction ratio and annealed at 1423 K for 10 min.

In case the annealing time is too short, *e.g.*, for the specimen cold-rolled at 5% reduction ratio and annealed at 1423 K for 5 min, the ratio of $(\sum 9 + \sum 27)/\sum 3$ is just 0.04, and the proportion of low $\sum$ CSL grain boundaries is much lower than that in the BM, indicating that GBCD of the specimen cold-rolled at 5% reduction ratio and annealed at 1423 K for 5 min is not truly optimized. This is because the recrystallization has not completed in this specimen, and most of $\sum 3$ grain boundaries are still coherent $\sum 3$ twin boundaries (Fig. 4(a)), for which it is very difficult to migrate and react with the other grain boundaries[25]. In other words, the deriving capacity of these coherent $\sum 3$ twin boundaries to $\sum 9$ and $\sum 27$ ones is very weak. Accordingly, the proportion of low CSL grain boundaries is quite low and the optimization effect is not achieved in the specimen cold-rolled at 5% reduction ratio and annealed at 1423 K for 5 min. On the contrary, the $\sum 3$, $\sum 9 + \sum 27$ and the ratio of $(\sum 9 + \sum 27)/\sum 3$ are the highest in the specimen cold-rolled at 5% reduction ratio and annealed at 1423 K for 10 min. That is to say, the GBCD optimization effect is the best under this GBE process.

5. Conclusions

An HNASS containing 0.63% nitrogen produced by a pressurized ESR process was thermomechanical-processed for GBE. The following concluding remarks can be drawn.

The optimization process of GBE in conventional ASS cannot be well applied to the present HNASS. A GBE process involving 5% cold-rolling reduction followed by annealing at 1423 K for 10 min is the most feasible for the optimization of GBCD in HNASS under the current experimental conditions. By this way, the fraction of low $\sum$ CSL grain boundaries could be increased from 47.3% to 82.0%. These special boundaries of high proportion can effectively interrupt the connectivity of conventional HABs network, achieving the anticipated effect of GBCD optimization for HNASS.

Acknowledgements

This work was supported by National Natural Science Foundation of China (Nos. 51201027 and 51271054) and Fundamental Research Funds for the Central Universities of China (Nos. N110105001, N120405001 and N120505001).

REFERENCES

[1] M. Diener and M.O. Speidel, Mater. Manuf. Processes **19** (2004) 111.
[2] Z.Z. Yuan, Q.X. Dai, X.N. Cheng, K.M. Chen and W.W. Xu, Mater. Sci. Eng. A **475** (2008) 202.
[3] H. Hänninen, J. Romu, R. Ilola, J. Tervo and A. Laitinen, J. Mater. Process. Technol. **117** (2001) 424.
[4] D. López, N.A. Falleiros and A.P. Tschiptschin, Wear **263** (2007) 347.
[5] G. Stein, I. Hucklenbroich and M. Wagner, Mater. Sci. Forum **318–320** (1999) 167.
[6] M. Ogawa, K. Hiraoka, Y. Katada, M. Sagara and S. Tsukamoto, ISIJ Int. **42** (2002) 1391.
[7] P.H. Pumphrey, In: G.A. Chadwick and D.A. Smith

(Eds.), Special High Angle Boundaries, Grain Boundary Structure and Properties, Academic Press, London, 1976, pp.13–19.
[8] X.Y. Fang, K. Zhang, H. Guo, W.G. Wang and B.X. Zhou, Mater. Sci. Eng. A **487** (2008) 7.
[9] X.Y. Fang, W.G. Wang, Z.X. Cai, C.X. Qin and B.X. Zhou, Mater. Sci. Eng. A **527** (2010) 1571.
[10] C.L. Hu, S. Xia, H. Li, T.G. Liu, B.X. Zhou, W.J. Chen and N. Wang, Corros. Sci. **53** (2011) 1880.
[11] Y. Wang, J. Kaneda and N. Shigenaka, Corros. Eng. **60** (2011) 141.
[12] M. Shimada, H. Kokawa, Z.J. Wang, Y.S. Sato and I. Karibe, Acta Mater. **50** (2002) 2331.
[13] M. Michiuchi, H. Kokawa, Z.J. Wang, Y.S. Sato and K. Sakai, Acta Mater. **54** (2006) 5179.
[14] R. Valerie and J. Richard, Mater. Sci. Eng. A **524** (2009) 134.
[15] O.V. Mishin, V.Y. Gertsman, I.V. Alexandrov and R.Z. Valiev, Mater. Sci. Eng. A **212** (1996) 281.
[16] K. Shigeaki, H. Masashi, T. Sadahiro and W. Tadao, Procedia Eng. **10** (2011) 112.
[17] B. Ravi Kumar, S. K. Das, B. Mahato, A.Das and S. Ghosh Chowdhury, Mater. Sci. Eng. A **454–455** (2007) 239.
[18] M. Sekine, N. Sakaguchi, M. Endo, H. Kinoshita, S. Watanabe, H. Kokawa, S. Yamashita, Y. Yano and M. Kawai, J. Nucl. Mater. **414** (2011) 232.
[19] E.A. West and G.S. Was, J. Nucl. Mater. **392** (2009) 264.
[20] J.A. Basinger, E.R. Homer, D.T. Fullwood and B.L. Adams, Scr. Mater. **53** (2005) 959.
[21] S.H. Kim, U. Erb, K.T. Aust and G. Palumbo, Scr. Mater. **44** (2001) 835.
[22] V.Y. Gertsman, M. Janecek and K. Tangri, Acta Mater. **44** (1996) 2869.
[23] F. Shi, X.W. Li, Y. Qi and C.M. Liu, Steel Res. Int. (2013). (in press)
[24] H. Kokawa, W.Z. Jin, Z.J. Wang, M. Michiuchi, Y.S. Sato, W. Dong and Y. Katada, Mater. Sci. Forum **539–543** (2007) 4962.
[25] W.G. Wang and B.X. Zhou, in: the 11th procceding of Chinese Stereology and Image Analysis, Chinese Society for Stereology, Ningbo, China, October 17–21, 2006. (in Chinese)
[26] V. Randle, Acta Mater. **52** (2004) 4067.
[27] M. Kumar, A.J. Schwartz and W.E. King, Acta Mater. **50** (2002) 2599.